Design of Optimal Control of DFIG-based Wind Turbine System through Linear Quadratic Regulator

Ines Zgarni, Lilia ElAmraoui
Research Laboratory Smart Electricity & ICT, SE&ICT Lab., LR18ES44
National School of Engineers of Carthage
University of Carthage, Tunisia

***Abstract*—This paper is devoted to implement an optimal control approach applying Linear Quadratic Regulator (LQR) to control a DFIG based Wind Turbine. The main goal of proposed LQR Controller is to achieve the active and reactive power and the DC-link voltage control of DFIG system in order to extract the maximum power from the wind turbine. In fact, the linearized state-space model of studied system in the d-q rotating reference frame is established. However, the overall system is controlled using MPPT strategy. The simulation results are obtained with Sim-Power-System and Simulink of MATLAB in terms of steady-state values, Peak amplitude, settling time and rise-time. Finally, the eigenvalue analysis and the simulation results are rated to ensure studied system robustness and stability, and the effectiveness of the control strategy.**

***Keywords*—Wind turbine system; doubly fed induction generator; DFIG; optimal control; linear quadratic regulator; LQR**

I. Introduction

The main renewable energy sources are Hydro Energy, Wind Energy (onshore or offshore), Solar Energy (PV or thermal), Biomass, Geothermal Energy, Wave Energy, Tidal Energy, and other alternative sources [1].

In 2020, according to IRENA (International Renewable Energy Agency), the share of renewable energy of global electricity production reached 36.6% which 9.58% produced by Wind energy [2][3].

Nowadays, due to the importance that takes the energy, which is at the core of all economic activity, the massive integration of wind turbine systems on power grids has created an effervescence in the world of scientific research, thus making it possible to improve the performance of wind turbines in terms of efficiency, reduced overall costs and maximum extraction energy [4].

In fact, many research works have been established studying the development of new design and control approaches for wind power system.

The most common combination for wind turbines is that with variable speed (with wide range of operation) and based on Doubly Fed Induction Generator (DFIG) which offers 10-15% higher wind energy capture and holds flexible control [5].

In the literature, Vector control is generally applied to control active and reactive powers of DFIG [6]. Even if, over the last three decades, the PI controller is the most successful controllers mostly in the 1st order SISO model of DFIG. Nevertheless, facing variation of DFIG's parameters (MIMO system), PI becomes vulnerable. [7].

This research work stands out an LQR regulator, as a feedforward controller, using a linearized state-space model of the DFIG wind turbine. This approach reaches zero error between the desired magnitudes and the measured ones for the active and reactive powers and the DC-link voltage within a considerable time delay.

This paper is structured as follows. Section II presents related works. Section III describes the equivalent circuit of wind turbine based on DFIG and the modeling of the wind turbine, the DFIG, the grid side filter and the DC-link in d-q rotating reference frame. Section IV presents the linearized system around a point of equilibrium. In Section V, an LQR control strategy for studied system is discussed. Section VI is devoted to the implementation by creating a block diagram by MATLAB Simulink. Section VII details the simulation of studied system and the obtained results. Section VIII concludes the paper. Finally, Section IX details system parameters.

II. Literature Review

In recent years, many works have been established on linear control of DFIG Based wind energy conversion system.

A direct control power output for DFIG wind turbine using LQR regulator for rotor side and grid side converters is evoked and discussed in [8].

A LQR Robust static state tracking control, described in [9], is designed to ensure tracking of the active and reactive power of the WECS over the wind speed range employing a polytopic LPV DFIG model.

In [10] they opted to use two control loops; from the reference power, the outer loop determines the reference rotor current and the interloop regulates the rotor current according to the outer loop output using LQR.

In this respect, in this paper, LQR Controller approach is proposed to improve the stability and robustness of the linearized DFIG system.

III. DFIG-Wind Turbine System Modeling

The aim of this section is to present the Overall system which explains the configuration of the doubly fed induction generator (DFIG) wind turbine.

At first sight, Gearbox establishes the connection between wind generator (DFIG) and wind turbine [11]. Then, the stator is directly connected to the grid, whereas the rotor is connected to the grid via back-to-back converter (RSC and GSC) [12].

Rotor-side-Converter (RSC) represents a rectifier which transforms AC currents and voltages delivered by the rotor into DC currents and voltages, thus allowing a decoupled control of the active and reactive powers [13].

However, GSC stands for a PWM controlled inverter that recuperates DC current and voltage at the output of RSC to generate a three phase AC current and voltage system with the same frequency as the grid given that the variation of the speed of the rotor according to the speed of the wind generates a current with variable frequency.

This configuration allows variable speed operation of wind turbines [14].

Fig. 1 shows general configuration of Wind Turbine system based on DFIG. At the beginning, each part is modeled separately.

A. *The Model of Wind Turbine*

Given that the static characteristics of a wind turbine rotor are derived from the relationships between the total wind power and the mechanical power of the wind turbine.

Some parameters of the variable speed wind turbine are taken into consideration in order to modeling DFIG.

In this study, turbine angular speed is considered equal to generator angular speed. Thus, system analysis and modeling have been done as a one-mass.

In Addition, the pitch angle controller dynamics is not taken into consideration on account of the fact that its slower response compared to the electrical control dynamics. Then, differential equation 1 reveals the rotation equation.

$$\frac{d\omega_r}{dt} = \frac{1}{2H}T_m - \frac{1}{2H}T_e \quad (1)$$

Where, ω_r : Generator angular speed; H: total equivalent inertia (the equivalent inertia reduced to the shaft); Tm: Mechanical torque and Te: Electromagnetic torque.

The mechanical power captured by the WT is described as follows: [16]

$$P_m(t) = \frac{1}{2}\rho_{air}\pi R^2 C_p(\lambda, \beta){V_w}^3(t) \quad (2)$$

Where ρ_{air} identifies the air density, R is the blade radius, C_p denotes Power coefficient, and V_w represents the wind speed.

The power coefficient C_p depends essentially on two parameters which are β (Pitch angle of the blade) and λ (Tip sleep ratio).

λ is defined by the following expression: [17]

$$\lambda = \frac{R\omega_r}{V_w} \quad (3)$$

Thus, the curve describing the Power coefficient C_p as a function of the Tip sleep ratio λ by taking a fixed value of pitch angle of the blades β is given by Fig. 2.

As shown in Fig. 2, C_p has a maximum point to a specific value of λ equal to λ_{opt}.

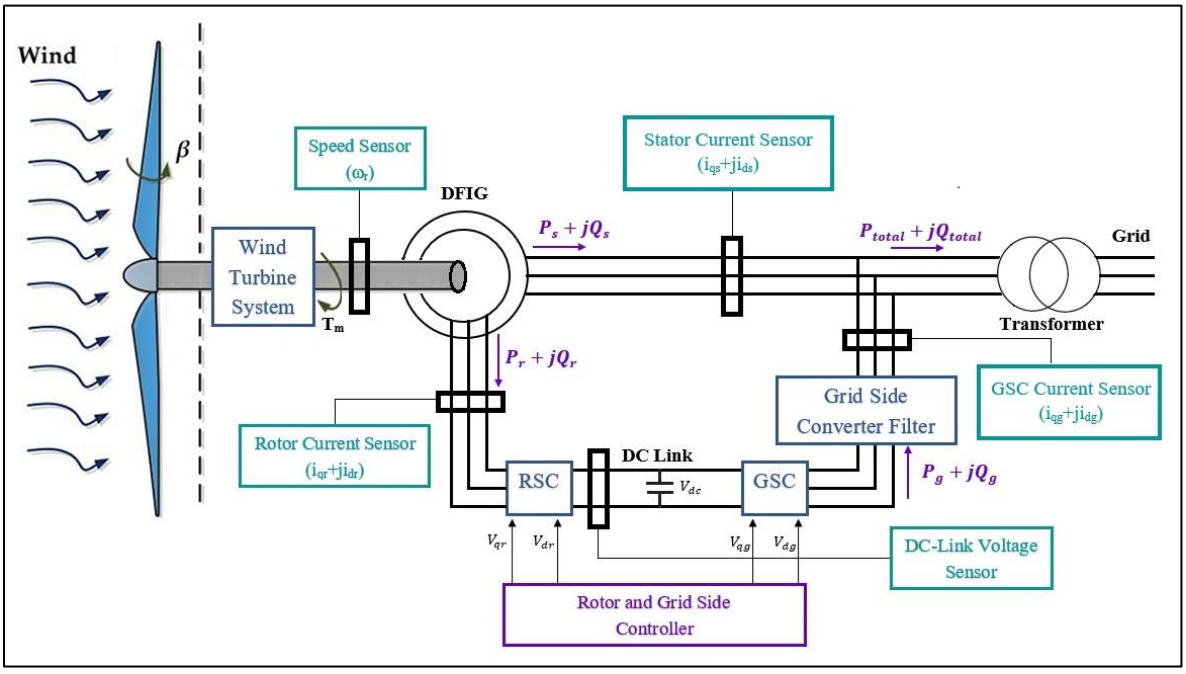

Fig. 1. General Configuration of Wind Turbine System based on DFIG. [15].

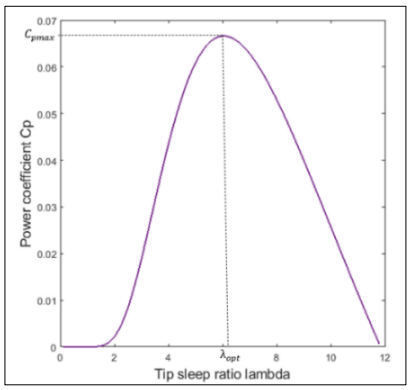

Fig. 2. Power Coefficient as a Function of the Tip Sleep Ratio.

Therefore, the expression of maximum mechanical power P_{max} is determined by equation 4. [18].

$$P_{max}(t) = \frac{1}{2}\rho_{air}\pi R^2 C_{pmax} {V_w}^3(t) \quad (4)$$

Furthermore, the range of the optimal power control for WT is obtained when: $\omega_r \in [\omega_{rmin}, \omega_{rrated}]$ and $V_w \in [V_{wmin}, V_{wrated}]$.

The control system for wind turbines is generally operates according to the technique of MPPT (Maximum Power Point Tracking). Then, the equation 5 represents the turbine power and the mechanical torque [19], [20].

$$P_{MPPT} = K_{opt}{\omega_r}^3 \text{ and } T_m = K_{opt}{\omega_r}^2 \quad (5)$$

With: $K_{opt} = \frac{1}{2}\rho\pi R^5 \frac{C_{pmax}}{{\lambda_{opt}}^3}$ [21]

In fact, the electromagnetic torque is obtained by making the ratio of air gap power to the DFIG mechanical speed. it is then written in the form:

$$T_e = L_m i_{qs} i_{dr} - L_m i_{ds} i_{qr} \quad (6)$$

To sum up, the rate of change of the generator angular speed is obtained from equations 1, 5 and 6.

$$\frac{d\omega_r}{dt} = \frac{K_{opt}}{2H}{\omega_r}^2 - \frac{L_m}{2H} i_{qs} i_{dr} + \frac{L_m}{2H} i_{ds} i_{qr} \quad (7)$$

B. DFIG Model

The DFIG is described in the dq frame as follows: the equations describing DFIG in dq frame are as follows: [22]

$$V_{ds} = -R_s i_{ds} - \omega_s \Psi_{qs} - \frac{1}{\omega_B}\frac{d(\psi_{ds})}{dt} \quad (8)$$

$$V_{qs} = -R_s i_{qs} + \omega_s \Psi_{ds} - \frac{1}{\omega_B}\frac{d(\psi_{qs})}{dt} \quad (9)$$

$$V_{dr} = -R_r i_{dr} - (\omega_s - \omega_r)\Psi_{qr} - \frac{1}{\omega_B}\frac{d(\psi_{dr})}{dt} \quad (10)$$

$$V_{qr} = -R_r i_{qr} + (\omega_s - \omega_r)\Psi_{dr} - \frac{1}{\omega_B}\frac{d(\psi_{qr})}{dt} \quad (11)$$

With:

$$\psi_{ds} = L_{ss} i_{ds} + L_m i_{dr} \quad (12)$$

$$\psi_{qs} = L_{ss} i_{qs} + L_m i_{qr} \quad (13)$$

$$\psi_{dr} = L_m i_{ds} + L_{rr} i_{dr} \quad (14)$$

$$\psi_{qr} = L_m i_{qs} + L_{rr} i_{qr} \quad (15)$$

And

$$L_{ss} = L_s + L_m \quad (16)$$

$$L_{rr} = L_r + L_m \quad (17)$$

Where (V_{ds}, V_{qs}) and (V_{dr}, V_{qr}) represents stator and rotor voltages in dq frame, respectively; (i_{ds}, i_{qs}) and (i_{dr}, i_{qr}) denotes stator and rotor currents in dq frame, respectively; (ψ_{ds},ψ_{qs}) and (ψ_{dr},ψ_{qr}) identifies stator and rotor flux in dq frame, respectively; L_{ss} and L_{rr} stands for stator and rotor self-inductance, respectively; (L_s, R_s) represents stator leakage inductance and resistance; (L_r, R_r) represents rotor leakage inductance and resistance; L_m is an abbreviation for mutual inductance; at last, ω_s identifies synchronous angular speed.

Moreover, the base speed is taken equal to $\omega_B = 2\pi f$ with $f = 50\ Hz$ which represents nominal frequency. [23]

The rotor slip is determined as follows:

$$s = 1 - \frac{\omega_r}{\omega_s} \quad (18)$$

Section 8.1 includes all constant parameters of studied system.

From the equations 8 to 17, the rate change of rotor and stator current in dq frame is established [24].

$$\frac{di_{qs}}{dt} = \left(\frac{\omega_B R_s L_{rr}}{{L_m}^2 - L_{ss}L_{rr}}\right) i_{qs} + \left(\frac{\omega_B}{{L_m}^2 - L_{ss}L_{rr}}\right)\left[(\omega_s - \omega_r){L_m}^2 - \omega_s L_{ss} L_{rr}\right] i_{ds} - \left(\frac{\omega_B R_r L_m}{{L_m}^2 - L_{ss}L_{rr}}\right) i_{qr} + \left(\frac{\omega_B}{{L_m}^2 - L_{ss}L_{rr}}\right)\left[(\omega_s - \omega_r)L_m L_{rr} - \omega_s L_m L_{rr}\right] i_{dr} - \left(\frac{\omega_B L_m}{{L_m}^2 - L_{ss}L_{rr}}\right) V_{qr} + \left(\frac{\omega_B L_{rr}}{{L_m}^2 - L_{ss}L_{rr}}\right) V_{qs} \quad (19)$$

$$\frac{di_{ds}}{dt} = \left(\frac{\omega_B}{{L_m}^2 - L_{ss}L_{rr}}\right)\left[\omega_s L_{ss} L_{rr} - (\omega_s - \omega_r){L_m}^2\right] i_{qs} + \left(\frac{\omega_B R_s L_{rr}}{{L_m}^2 - L_{ss}L_{rr}}\right) i_{ds} - \left(\frac{\omega_B R_r L_m}{{L_m}^2 - L_{ss}L_{rr}}\right) i_{dr} + \left(\frac{\omega_B}{{L_m}^2 - L_{ss}L_{rr}}\right)\left[\omega_s L_m L_{rr} - (\omega_s - \omega_r)L_m L_{rr}\right] i_{qr} - \left(\frac{\omega_B L_m}{{L_m}^2 - L_{ss}L_{rr}}\right) V_{dr} + \left(\frac{\omega_B L_{rr}}{{L_m}^2 - L_{ss}L_{rr}}\right) V_{ds} \quad (20)$$

$$\frac{di_{qr}}{dt} = -\left(\frac{\omega_B R_s L_m}{{L_m}^2 - L_{ss}L_{rr}}\right) i_{qs} + \left(\frac{\omega_B}{{L_m}^2 - L_{ss}L_{rr}}\right)\left[\omega_s L_m L_{ss} - (\omega_s - \omega_r)L_m L_{ss}\right] i_{ds} + \left(\frac{\omega_B R_r L_{ss}}{{L_m}^2 - L_{ss}L_{rr}}\right) i_{qr} + \left(\frac{\omega_B}{{L_m}^2 - L_{ss}L_{rr}}\right)\left[\omega_s {L_m}^2 - (\omega_s - \omega_r)L_{ss} L_{rr}\right] i_{dr} + \left(\frac{\omega_B L_{ss}}{{L_m}^2 - L_{ss}L_{rr}}\right) V_{qr} + \left(\frac{\omega_B L_m}{{L_m}^2 - L_{ss}L_{rr}}\right) V_{qs} \quad (21)$$

$$\frac{di_{dr}}{dt} = \left(\frac{\omega_B}{{L_m}^2 - L_{ss}L_{rr}}\right)\left[(\omega_s - \omega_r)L_m L_{ss} - \omega_s L_m L_{ss}\right] i_{qs} - \left(\frac{\omega_B R_s L_m}{{L_m}^2 - L_{ss}L_{rr}}\right) i_{ds} + \left(\frac{\omega_B R_r L_{ss}}{{L_m}^2 - L_{ss}L_{rr}}\right) i_{dr} + \left(\frac{\omega_B}{{L_m}^2 - L_{ss}L_{rr}}\right)\left[(\omega_s - \omega_r)L_{ss} L_{rr} - \omega_s {L_m}^2\right] i_{qr} + \left(\frac{\omega_B L_{ss}}{{L_m}^2 - L_{ss}L_{rr}}\right) V_{dr} - \left(\frac{\omega_B L_m}{{L_m}^2 - L_{ss}L_{rr}}\right) V_{ds} \quad (22)$$

C. The Model of the Grid-side Filter

As it is known that the GSC serves to stabilize DC voltage by supervising the power transition in the grid, whereas the GSC filter is employed to minimize the system harmonics as well as to adjust the phase and amplitude of the voltage in the output of the GSC [25].

The circuit corresponding to the GSC Filter is given by Fig. 3.

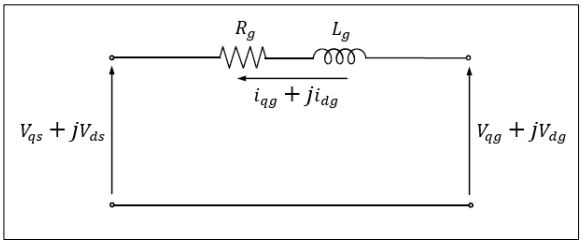

Fig. 3. GSC Filter Equivalent Circuit.

Where R_g and L_g identifies the resistance and the inductance of the Grid side filter, respectively, and (i_{dg}, i_{qg}) and (V_{dg}, V_{qg}) stands for the GSC current and voltage components, respectively. [26].

Furthermore, the GSC current are given as follows:

$$\frac{di_{qg}}{dt} = -\frac{\omega_B R_g}{L_g} i_{qg} + \omega_B \omega_s i_{dg} + \frac{\omega_B}{L_g} V_{qg} - \frac{\omega_B}{L_g} V_{qs} \quad (23)$$

$$\frac{di_{dg}}{dt} = -\omega_B \omega_s i_{qg} - \frac{\omega_B R_g}{L_g} i_{dg} + \frac{\omega_B}{L_g} V_{dg} - \frac{\omega_B}{L_g} V_{ds} \quad (24)$$

D. The Model of DC-Link

The two converters of the wind energy conversion system (RSC and GSC) are interconnected via a DC-link capacitor which allows energy storage.

Acting as a reactive power source, the rotor-side magnetizing current is supplied by DC-link. Otherwise, the control of the stator-side power factor can be established.

In this study, supposing that the losses of the converter are neglected, the active power of DC-link P_{DC} is determinate as follows:

$$P_{DC} = P_r - P_g \quad (25)$$

Where P_g and P_r identifies the active power at the RSC and GSC AC terminal, respectively.

It is also written in this form:

$$P_{DC} = V_{DC} i_{DC} = V_{DC} C_{DC} \frac{dV_{DC}}{dt} \quad (26)$$

Where V_{DC} and i_{DC} are the voltage across DC-link capacitor and the current flowing through the capacitor, respectively.

The derivative of V_{DC} is, thus, obtained as a function of P_g and P_r.

$$\frac{dV_{DC}}{dt} = \frac{1}{C_{DC} V_{DC}} \left(P_r - P_g\right) \quad (27)$$

Moreover, by calculating the apparent power, the stator active power P_s represents real part of equation 28. As for the stator reactive power Q_s, it denotes the imaginary part.

$$P_s + jQ_s = V_{dqs} {i_{dqs}}^* = \left(V_{qs} + jV_{ds}\right)\left(i_{qs} + ji_{ds}\right)^* \quad (28)$$

Accordingly, the expressions of P_s and Q_s are given by equations 29 and 30. [27].

$$P_s = \left[V_{qs} i_{qs} + V_{ds} i_{ds}\right] \quad (29)$$

$$Q_s = \left[V_{ds} i_{qs} - V_{qs} i_{ds}\right] \quad (30)$$

Based on the same principle, the rotor active and reactive powers can be obtained as follows: [28].

$$P_r = \left[V_{qr} i_{qr} + V_{dr} i_{dr}\right] \quad (31)$$

$$Q_r = \left[V_{dr} i_{qr} - V_{qr} i_{dr}\right] \quad (32)$$

Similarly, the active and reactive power, on the Grid-side converter, is given by equations 33 and 34.

$$P_g = \left[V_{qg} i_{qg} + V_{dg} i_{dg}\right] \quad (33)$$

$$Q_g = \left[V_{dg} i_{qg} - V_{qg} i_{dg}\right] \quad (34)$$

Then, by exploiting the equations 27 to 34, the expression of $\frac{dV_{DC}}{dt}$ becomes as follows:

$$\frac{dV_{DC}}{dt} = \frac{1}{C_{DC} V_{DC}} \left(V_{qr} i_{qr} + V_{dr} i_{dr} - V_{qg} i_{qg} - V_{dg} i_{dg}\right) \quad (35)$$

IV. Studied System Linearization

The dynamic characteristics of the studied system will be analyzed by studying the different linearization techniques and eigenvalues.

The modeling of the whole of the studied system comprising DFIG, GSC filter, and the subsystem of drive train is obtained by combining the models of the above-mentioned subsystems.

The small-signal model is established revealing linearization around operating point:

$$\left(i_{qs0}, i_{ds0}, i_{qr0}, i_{dr0}, i_{qg0}, i_{dg0}, \omega_{r0}, V_{DC0}\right)$$

Moreover, q axis of the machine is set in such a way that it coincides with stator voltage V_s. Consequently, the total voltage corresponds to q-axis stator voltage ($V_s = V_{qs}$) and d-axis stator voltage is taken zero ($V_{ds} = 0$).

The generalized equations are written as follows: [29]

$$\dot{x} = f(x, y) \quad (36)$$

$$y = g(x, y) \quad (37)$$

Vectors x, y and u represent the state vector, the output vector, and the control vector respectively. f and g denote nonlinear functions.

The equations of the state-space are as follows: [30]

$$\Delta\dot{x} = A\Delta x + B\Delta u \quad (38)$$

$$\Delta y = C\Delta x + D\Delta u \quad (39)$$

With Δ stands for the deviation. Thus, the deviations of the state, input and output variables are given by equations 40, 41, and 42.

$$\Delta x = [\Delta i_{qs} \quad \Delta i_{ds} \, \Delta i_{qr} \quad \Delta i_{dr} \quad \Delta i_{qg} \, \Delta i_{dg} \quad \Delta \omega_r \quad \Delta V_{DC}]^T \tag{40}$$

$$\Delta u = [\Delta V_{qr} \quad \Delta V_{dr} \, \Delta V_{qg} \quad \Delta V_{dg}]^T \tag{41}$$

$$\Delta y = [\Delta P_s \quad \Delta Q_s \quad \Delta P_r \, \Delta Q_r \quad \Delta P_g \, \Delta Q_g \quad \Delta V_{DC}]^T \tag{42}$$

The matrices A, B, C and D which stand for respectively the state matrix, the control matrix, output matrix and feedforward matrix are computed and shown in equations 43, 46.

$$A = \begin{bmatrix} A_{11} & A_{12} & A_{13} & A_{14} & A_{15} & A_{16} & A_{17} & A_{18} \\ A_{21} & A_{22} & A_{23} & A_{24} & A_{25} & A_{26} & A_{27} & A_{28} \\ A_{31} & A_{32} & A_{33} & A_{34} & A_{35} & A_{36} & A_{37} & A_{38} \\ A_{41} & A_{42} & A_{43} & A_{44} & A_{45} & A_{46} & A_{47} & A_{48} \\ A_{51} & A_{52} & A_{53} & A_{54} & A_{55} & A_{56} & A_{57} & A_{58} \\ A_{61} & A_{62} & A_{63} & A_{64} & A_{65} & A_{66} & A_{67} & A_{68} \\ A_{71} & A_{72} & A_{73} & A_{74} & A_{75} & A_{76} & A_{77} & A_{78} \\ A_{81} & A_{82} & A_{83} & A_{84} & A_{85} & A_{86} & A_{87} & A_{88} \end{bmatrix} \tag{43}$$

All the elements of matrix A are given in section 8.2.

$$B = \begin{bmatrix} \frac{-\omega_B L_m}{{L_m}^2 - L_{ss} L_{rr}} & 0 & 0 & 0 \\ 0 & \frac{-\omega_B L_m}{{L_m}^2 - L_{ss} L_{rr}} & 0 & 0 \\ \frac{\omega_B L_{ss}}{{L_m}^2 - L_{ss} L_{rr}} & 0 & 0 & 0 \\ 0 & \frac{\omega_B L_{ss}}{{L_m}^2 - L_{ss} L_{rr}} & 0 & 0 \\ 0 & 0 & \frac{\omega_B}{L_g} & 0 \\ 0 & 0 & 0 & \frac{\omega_B}{L_g} \\ 0 & 0 & 0 & 0 \\ \frac{i_{qr0}}{C_{DC} V_{DC0}} & \frac{i_{dr0}}{C_{DC} V_{DC0}} & \frac{-i_{qg0}}{C_{DC} V_{DC0}} & \frac{-i_{dg0}}{C_{DC} V_{DC0}} \end{bmatrix} \tag{44}$$

$$C = \begin{bmatrix} V_{qs0} & V_{ds0} & 0 & 0 & 0 & 0 & 0 & 0 \\ V_{ds0} & -V_{qs0} & 0 & 0 & 0 & 0 & 0 & 0 \\ 0 & 0 & V_{qr0} & V_{dr0} & 0 & 0 & 0 & 0 \\ 0 & 0 & V_{dr0} & -V_{qr0} & 0 & 0 & 0 & 0 \\ 0 & 0 & 0 & 0 & V_{qg0} & V_{dg0} & 0 & 0 \\ 0 & 0 & 0 & 0 & V_{dg0} & -V_{qg0} & 0 & 0 \\ 0 & 0 & 0 & 0 & 0 & 0 & 0 & 1 \end{bmatrix} \tag{45}$$

$$D = \begin{bmatrix} 0 & 0 & 0 & 0 & i_{qs0} & i_{ds0} \\ 0 & 0 & 0 & 0 & -i_{ds0} & i_{qs0} \\ i_{qr0} & i_{dr0} & 0 & 0 & 0 & 0 \\ -i_{dr0} & i_{qr0} & 0 & 0 & 0 & 0 \\ 0 & 0 & i_{qg0} & i_{dg0} & 0 & 0 \\ 0 & 0 & -i_{dg0} & i_{qg0} & 0 & 0 \\ 0 & 0 & 0 & 0 & 0 & 0 \end{bmatrix} \tag{46}$$

V. LQR Controller Design

Modeling the small signal is set in order to apply the control law: $u = -K_{LQR} x$. The control law is determined by minimizing the LQR cost function given by equation 47. [31].

$$J = \int_0^\infty (x^T Q x + u^T R u) dt \tag{47}$$

Where Q (8×8) and R (4×4) denotes the state and control weighting matrices. They are symmetric and square.

Besides, in this study, Q and R are chosen as identity matrices.

As a result of the theory of linear control, matrix gain K_{LQR} is obtained as follows:

$$K_{LQR} = R^{-1} B^T P \tag{48}$$

Where P (positive-definite matrix) is spotted by solving the following continuous Riccati equation: [32].

$$A^T P + P A - P B R^{-1} B^T P + Q = 0 \tag{49}$$

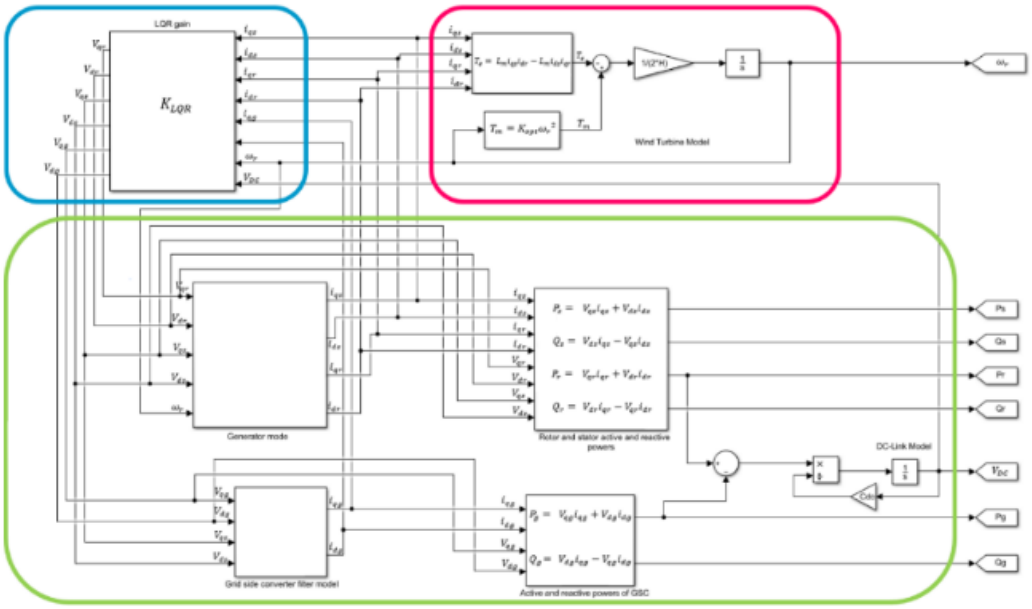

Fig. 4. Block Diagram of Studied System Simulation.

In fact, K_{LQR} is determined by ensuring the stability of the system. The checks carried out are as follows:

The controllability of (A, B) and the observability of (Q, A),

$(A - BK_{LQR})$ which represents the closed-loop system must be asymptotically stable, that is, accomplished by checking the matrix eigenvalues that they must have a negative real part.

The step response of studied system is detailed in Section 5 after identifying the feedback LQR gain K_{LQR} which is detailed in Section 8.3.

Given that the cost function J represent the integral summing of the control effort J_u and the criterion of performance J_x illustrated by equations 50 and 51.

$$J_u = \left(V_{qr}\right)^2 + (V_{dr})^2 + \left(V_{qg}\right)^2 + \left(V_{dg}\right)^2 \quad (50)$$

$$J_x = \left(i_{qs}\right)^2 + (i_{ds})^2 + \left(i_{qr}\right)^2 + (i_{dr})^2 + \left(i_{qg}\right)^2 + \left(i_{dg}\right)^2 + (\omega_r)^2 + (V_{DC})^2 \quad (51)$$

VI. Implementation of Studied System

The Fig. 4 shows the block diagram of studied system simulation, which is accomplished using Simulink of MATLAB, the help of Sim power System and the built-in LQR function of MATLAB.

According to Fig. 4, the overall operational diagram of studied system is described as follows: the blue box presents the proposed LQR controller algorithm, the pink box indicates the wind turbine model, and the green box encompasses the DFIG model, the GSC Filter model and the DC-Link model.

VII. Simulation and Results

The studied system's response as achieved using previously detailed and discussed control algorithm, are described in this section.

The DFIG's overall characteristics and the location of the poles have been obtained in such a way that ensures the stability of the system.

Table I illustrate the DFIG's eigenvalues without and with proposed controller.

Without controller, the positive real part was identified for one eigenvalue that is providing the instability of the initial system. As shown in Table I, in case of proposed controller, all eigenvalues dispose negative real part.

TABLE I. DFIG'S EIGENVALUES WITHOUT AND WITH PROPOSED CONTROLLER

Without LQR controller	With LQR Controller
-16.2 ± 313.5i	-13963.6 ± 314i
-4.8	-4429 ± 94.25i
-14.4 ± 120i	-1.4 + 314i
-167.5 ± 314i	-9.2
+0.00000071	-1.3

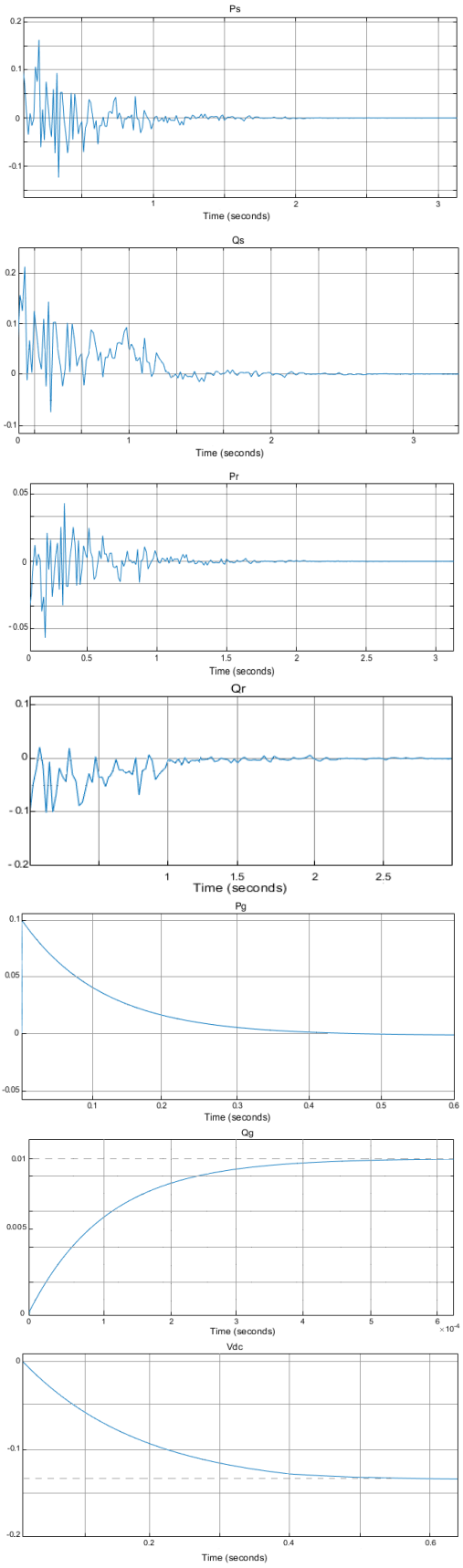

Fig. 5. Output Variables Errors with Proposed Control Approach.

From the simulation, the active and reactive powers, the DC-Link voltage, and the generator angular speed have been determined.

To sum up, the following specifications of time-domain, given by Table II, have been obtained from Fig. 5.

TABLE II. (A) SPECIFICATIONS OF TIME-DOMAIN

Output variables	P_s	Q_s	P_r	Q_r
Peak-value	-0.161pu	0.218pu	-0.186pu	-0.102pu
Rise-time	7.39e-04s	0.001 s	1.1e-04 s	1.6e-04 s
Settling time	2.37s	2.77 s	0.112 s	2.77 s
Steady-state-value	-0.078pu	0.0193pu	-0.021pu	0.004 pu

(B) SPECIFICATIONS OF TIME-DOMAIN

Output variables	P_g	Q_g	V_{DC}
Peak-value	0.09 pu	0.01 pu	-0.131 pu
Rise-time	0.403 s	2.19e-04 s	0.238 s
Settling time	0.576 s	0.54e-04 s	0.52 s
Steady-state-value	-0.002 pu	0.01 pu	-0.131 pu

Previously, the simulation results described are satisfactory in terms of Peak-value, rise-time and settling time.

Given that the evaluation of optimization problems without constraints is a primary objective of an LQR controller.

However, the proposed controller ensures a systematic computation of the state feedback gain matrix as well as a regulation of all the states to zero which is validated by the values of steady-state found for the active and reactive powers and the DC-Link voltage.

VIII. CONCLUSION

In this paper, the design, and the implementation of LQR controller as a feedforward controller employing a linearized state-space model of the DFIG wind turbine in the rotating dq reference frames, is achieved in order to control the active and reactive powers and the DC-link voltage.

Further, the choice of the weighting matrices R and Q is focused on the investigation of a satisfactory response of the simulation.

According to the simulation results, with proposed controller, errors between the actual and desired values converged to zero and the response of the system shows good performance.

Finally, given that the LQR criterion can be perceived as a compromise between performance (described by the state weighting matrix Q) and consumption (denoted by the control weighting matrix R), the choice of the matrices R and Q (other than identity matrices) will be investigated in the forthcoming studies. Furthermore, comfortable stability margins will be determined to guarantee the robustness of the control.

IX. SYSTEM PARAMETERS

Simulations are obtained with a 7.5kW generator connected to a 220V/50Hz grid.

A. Parameters of Studied System and Steady State

The machine and steady-state parameters are illustrated in Table III.

TABLE III. PARAMETERS OF STUDIED SYSTEM AND STEADY STATE

Parameter	Designation	Value
ω_B	Base speed	314.16 rad/s
ω_s	Synchronous angular speed	1 pu
s	Rotor slip	-0.03
R_s	Stator resistance	0.005 pu
R_r	Rotor resistance	0.0055 pu
H	Total inertia (Wind turbine + generator)	3.5s
L_m	Mutual inductance	2.25 pu
L_{ss}	Stator self-inductance	2.2725 pu
L_{rr}	Rotor self-inductance	2.2839 pu
L_g	GSC filter inductance	0.0225 pu
R_g	GSC filter resistance	0.012 pu
X_t	Transmission line resistance and reactance	0.0225 pu
k_{opt}	Constant corresponding to the maximum power coefficient	0.5787
C_{dc}	DC-link capacitor	0.0001 pu
V_{dc0}	Initial DC-link voltage	1200 V
P_{total}	Total active power	1 pu
V_s	Stator voltage	1 pu
V_r	Rotor voltage	$V_s/_n$ pu
V_B	Slack bus voltage	1 pu
n	Stator to rotor turns ratio	1.5
i_{qs0}	Initial stator currents in dq frame	0.9999
i_{ds0}		-0.0563
i_{qr0}	Initial rotor currents in dq frame	1.437e-04
i_{dr0}		0.0675
i_{qg0}	Initial GSC currents in dq frame	1.437e-04
i_{dg0}		0.0675
ω_{r0}	Initial generator angular speed	1.03
V_{qr0}	Initial rotor voltages in dq frame	0.6667
V_{dr0}		0
V_{qs0}	Initial stator voltages in dq frame	1
V_{ds0}		0
V_{qg0}	Initial voltages at the GSC terminal in dq frame	1.00000172
V_{dg0}		0.0008

B. Elements of Matrix A

$$A_{11} = \frac{\omega_B R_s L_{rr}}{{L_m}^2 - L_{ss}L_{rr}}\ ; A_{12} = \frac{\omega_B\left((\omega_s - \omega_{r0}){L_m}^2 - \omega_s L_{ss}L_{rr}\right)}{{L_m}^2 - L_{ss}L_{rr}}\ ;$$

$$A_{13} = \frac{-\omega_B R_r L_m}{{L_m}^2 - L_{ss}L_{rr}}\ ; A_{14} = \frac{\omega_B((\omega_s - \omega_{r0})L_m L_{rr} - \omega_s L_m L_{rr})}{{L_m}^2 - L_{ss}L_{rr}}$$

$$A_{15} = A_{16} = A_{18} = 0\ ; A_{17} = \left(\frac{-\omega_B {L_m}^2 i_{ds0}}{{L_m}^2 - L_{ss}L_{rr}}\right) - \left(\frac{\omega_B L_m L_{rr} i_{dr0}}{{L_m}^2 - L_{ss}L_{rr}}\right);$$

$$A_{21} = -A_{12}; A_{22} = A_{11}; A_{23} = -A_{14};$$

$$A_{24} = A_{13}\ ; A_{25} = A_{26} = A_{28} = 0;$$

$$A_{27} = \left(\frac{\omega_B {L_m}^2 i_{qs0}}{{L_m}^2 - L_{ss}L_{rr}}\right) + \left(\frac{\omega_B L_m L_{rr} i_{qr0}}{{L_m}^2 - L_{ss}L_{rr}}\right);\ A_{31} = \frac{-\omega_B R_s L_m}{{L_m}^2 - L_{ss}L_{rr}}\ ;$$

$$A_{32} = \frac{\omega_B(\omega_s L_m L_{ss} - (\omega_s - \omega_{r0})L_m L_{ss})}{{L_m}^2 - L_{ss}L_{rr}}\ ; A_{33} = \frac{\omega_B R_r L_{ss}}{{L_m}^2 - L_{ss}L_{rr}};$$

$$A_{34} = \frac{\omega_B(\omega_s {L_m}^2 - (\omega_s - \omega_{r0})L_{ss}L_{rr})}{{L_m}^2 - L_{ss}L_{rr}}\ ;$$

$$A_{35} = A_{36} = A_{38} = 0;\ A_{37} = \left(\frac{\omega_B L_m L_{ss} i_{ds0}}{{L_m}^2 - L_{ss}L_{rr}}\right) + \left(\frac{\omega_B L_{ss} L_{rr} i_{dr0}}{{L_m}^2 - L_{ss}L_{rr}}\right);$$

$$A_{41} = -A_{32}\ ; A_{42} = A_{31}\ ; A_{43} = \frac{\omega_B\left((\omega_s - \omega_{r0})L_{ss}L_{rr} - \omega_s {L_m}^2\right)}{{L_m}^2 - L_{ss}L_{rr}}\ ;$$

$$A_{44} = A_{33}\ ; A_{45} = A_{46} = A_{48} = 0\ ;$$

$$A_{47} = \left(\frac{-\omega_B L_m L_{ss} i_{qs0}}{{L_m}^2 - L_{ss}L_{rr}}\right) + \left(\frac{-\omega_B L_{ss} L_{rr} i_{qr0}}{{L_m}^2 - L_{ss}L_{rr}}\right);$$

$$A_{51} = A_{52} = A_{53} = A_{54} = A_{57} = A_{58} = 0\ ; A_{55} = \frac{-\omega_B R_g}{L_g}\ ;$$

$$A_{56} = \omega_B \omega_s\ ; A_{61} = A_{62} = A_{63} = A_{64} = A_{67} = A_{68} = 0\ ;$$
$$A_{65} = -A_{56}\ ; A_{66} = A_{55}\ ;$$

$$A_{71} = \frac{-L_m i_{dr0}}{2H}\ ; A_{72} = \frac{L_m i_{qr0}}{2H}\ ; A_{73} = \frac{L_m i_{ds0}}{2H}\ ; A_{74} = \frac{-L_m i_{qs0}}{2H}\ ;$$
$$A_{75} = A_{76} = A_{78} = 0\ ; A_{77} = \frac{\omega_{r0} K_{opt}}{H}\ ;$$

$$A_{81} = A_{82} = A_{87} = 0\ ; A_{83} = \frac{V_{qr0}}{C_{DC} V_{DC0}}\ ; A_{84} = \frac{V_{dr0}}{C_{DC} V_{DC0}}\ ;$$
$$A_{85} = \frac{-V_{qg0}}{C_{DC} V_{DC0}}\ ; A_{86} = \frac{-V_{dg0}}{C_{DC} V_{DC0}}\ ;$$

$$A_{86} = \frac{V_{dr0} i_{dr0} + V_{qr0} i_{qr0} - V_{dg0} i_{dg0} - V_{qg0} i_{qg0}}{C_{DC} {V_{DC}}^2}$$

C. Numerical Values of LQR Controller Gain

$$K_{LQR} = \begin{bmatrix} -3.9908 & 4.8113 & -5.3490 & 4.7635 & 0.0002 & -0.0000 & -0.0390 & -0.4281 \\ -4.8137 & -3.9730 & -4.7661 & -5.3307 & -0.0000 & 0.0000 & 0.6911 & 0.0166 \\ -0.0019 & 0.0370 & 0.0031 & 0.0366 & 0.9890 & -0.0000 & -0.1458 & -0.9035 \\ -0.0000 & 0.0010 & 0.0002 & 0.0010 & 0.0000 & 0.9880 & -0.0036 & -0.0219 \end{bmatrix}$$

REFERENCES

[1] N. A. Randriantsoa, A. H. Fakra, M. P. Ranjaranimaro, M. N. M. Rachdi, J. C. Gatina, "New Management Algorithms for Smart Electricity Network: Designing and Working Principles", Progress in Advanced Computing and Intelligent Engineering, pp. 671-682, 2021.

[2] M. P. Pablo-Romero, A. Sanchez-Braza, A. Galyan, "Renewable energy use for electricity generation in transition economies: Evolution, targets and promotion policies", Renewable and Sustainable Energy Reviews, vol.138, 110481, 2021.

[3] IRENA. Renewable capacity statistics 2021. Abu Dhabi: International Renewable Energy Agency; 2021.

[4] https://www.irena.org/publications/2021/March/Renewable-Capacity-Statistics-2021.

[5] A. Chehouri, R. Younes, A. Ilinca, J. Perron, "Review of performance optimization techniques applied to wind turbines", Applied Energy, vol. 142, pp. 361 -388, 2015.

[6] R. Kumar, K. Raahemifar, A. S. Fung, "A critical review of vertical axis wind turbines for urban applications", Renewable and Sustainable Energy Reviews, vol. 89, pp. 281-291, 2018.

[7] D. Zouheyr, L. Baghli, A. Boumediene, "Real-Time Emulation of a Grid-connected Wind Energy Conversion System Based Double Fed Induction Generator Configuration under Random Operationg Modes", European Journal of Electrical Engineering, vol. 23, pp. 207-219, 2021.

[8] K. Kim, H.-G. Kim, Y. Song, and I. Paek, "Design and Simulation of an LQR-PI Control Algorithm for Medium Wind Turbine", Energies, vol. 12, 2248, 2019.

[9] D. Chung Phan, T. H. Trinh, "Application of linear quadratic regulator to control directly power for DFIG wind turbine". Journal of Electrical systems, vol. 15-1, pp. 42-52, 2019.

[10] S. Salhi, S. Salhi, "LQR Robust control for active and reactive power tracking of a DFIG based WECS", International Journal of Advanced Computer Science and Applications, vol. 10-1, pp. 565-579, 2019.

[11] R. Bhushan, K. Chatterjee, "Mathematical modeling and control of DFIG-based wind energy system by using optimized linear quadratic regulator weight matrices". International Transaction on Electrical energy system, e. 2416, 2017.

[12] B. Subudhi, P. S. Ogeti, "Optimal preview stator voltage-oriented control of DFIG WECS", the institution of Engineering and technology, vol. 12, pp. 1004-1013, 2018.

[13] E. Chetouani, Y. Errami, A. Obbadi, S. Sahnoun, "Optimal tuning of PI controllers using adaptive particle swarm optimization for doubly-fed induction generator connected to the grid during a voltage dip", Bulletin of Electrical Engineering and Informatics, vol. 10-5, pp. 2367-2376, 2021.

[14] Y.-K. Wu, W.-H. Yang, "Different control strategies on the rotor side converter in DFIG-based wind turbines", 3rd International Conference on Power and Energy Systems Engineering, vol. 8-12, pp. 551-555, Japon, 2016.

[15] D. Xu, F. Blaabjerg, W. Chen, N. Zhu, "Advanced control of doubly fed induction generator for wind power systems", John Wiley & Sons, pp. 85-95, 2018.

[16] V. Yaramasu, B. Wu, "Model predictive control of wind energy conversion systems", John Wiley & Sons, pp. 405-406, 2017.

[17] S. B. Abul Kashem, M. E. H. Chowdhury, A. Khandakar, A. Jubaer, A. Azad, S. Nushrat, " Wind Power Integrationn with Smart Grid and Storage System: Prospects and Limitations", International Journal of Advanced Computer Science and Applications, vol. 11-5, pp. 552-569, 2020.

[18] E. Chetouani, A. Obbadi, S. Sahnoun, " Backstepping and indirect vector control for rotor side converter of doubly fed-induction generator with maximum power point tracking", Chapter, Digital Technologies and Applications, pp. 1711-1723, 2021.

[19] D.-C. Phan, S. Yamamoto, "Maximum Energy Output of a DFIG Wind Turbine Using an Improved MPPT-Curve Method", Energies, vol. 8, pp. 11718 – 11736, 2015.

[20] D. Ounnas, M. Ramdani, S. Chenikher, T. Bouktir, "A fuzzy tracking control design strategy for wind energy conversion system", International conference on Renewable Energy Research and Applications, Italy, 2015.

[21] T. Ghennam, "Supervision of a wind farm for its integration into the management of an electrical network, Contribution of multi-level converters to the adjustment of wind turbines based ondoubly fed induction machine", Doctoral thesis, Central School of Lille, pp. 66-68, 2011.

[22] A. Hammami, I. Saidi, D. Soudani, " Comparative Study of PMSG Controllers for Variable Wind Turbine Power Optimization", International Journal of Advanced Computer Science and Applications, vol. 9-8, pp. 239-246, 2018.

[23] B. Q. V. Ngo, P. Rodriguez-Ayerbe, S. Olaru, "Model Predictive Direct Power Control for doubly fed induction generator based wind turbines with three-level neutral-point clamped inverter", 42nd Annual Conference of the IEEE Industrial Electronics Society, Italy, 2016.

[24] A. J. Laafou, A. A. Madi, A. Addaim, A. Intidam, "Dynamic modeling and improved control of a grid-connected DFIG used in wind energy conversion systems", Mathematical Problems in Engineering, 2020.

[25] F. Blaabjerg, D. M. Ionel, "Renewable Energy Devices and Systems with Simulations in MATLAB and ANSYS", CRC Press, pp.213-221, 2017.

[26] J. Hu, Y. Huang, D. Wang, H. Yuan, X. Yuan, "Modeling of grid-connected DFIG-based wind turbines for DC-link voltage stability analysis", IEEE Transactions on sustainable energy, vol. 6, pp. 1325-1336, 2015.

[27] G. Abad, "Power Electronics and Electric Drives for Traction Applications", John Wiley & Sons, pp. 162-176, 2017.

[28] N. Gurung, R. Bhattarai, S. Kamalasadan, "Optimal linear-quadratic-integral controller design for doubly-fed induction generator", IEEE Power & Energy Society General Meeting, 2017.

[29] K. S. Islam, W. Shen, A. Mahmud, M. A. Chowdhury, J. Zhang, "Stability enhancement of DFIG wind turbine using LQR pitch control overrated wind speed", IEEE 11th Conference on Industrial Electronics and Applications, 2016.

[30] B. Mehta, P. Bhatt, V Pandya, "Small signal stability enhancement of DFIG based wind power system using optimized controllers' parameters", International Journal of Electrical Power and Energy Systems, vol. 70, pp. 70-82, 2015.

[31] H. Oktay Erkol, "Linear Quadratic Regulator Design for position control of an inverted pendulum by grey wolf optimizer", International Journal of Advanced Computer Science ans Applications, vol. 9, pp. 13-16, 2018.

[32] R. Bhushan, K. ChatteIjee, R. Shanka, "Comparison between GA-based LQR and Conventional LQR Control Method ofDFIG Wind Energy System", 3rd International Conference on Recent Advances in Information Technology, 2016.

[33] I.Zgarni, L. El Amraoui, "Study of optimal control applied to a Doubly Fed Induction Generator attached to wind turbine system", 6th IEEE International Energy Conference, pp. 511-514, 2020.